Radiative Characteristic of On-Chip Terahertz (THz) Structures

Yasser A. Hussein and James E. Spencer
Stanford Linear Accelerator Center, Stanford University
Menlo Park, CA 94025, U.S.A

Introduction

Previously, we explored possibilities for producing narrow-band THz radiation using either free or bound electrons (solid state) in micro-undulatory configurations [1] because integrated circuit technology appeared well matched to this region extending from about 300 GHz to 30 THz. This range [2]-[3] has largely been neglected until recently because it runs from the limit of WR-3 waveguide around 300 GHz up to CO_2 lasers where the laser regime becomes dominant. There are mainly two approaches for generating THz radiation, i.e. through free or bound electron (BE) implementations. In this paper, emphasis is on producing this radiation using bound electrons via IC technology but in close analogy to free electron lasers (FELs) that are comparatively immense, expensive, need high power and have low efficiencies [4].

General Discussion

It is useful to consider the analogy between the free case and the solid-state case proposed here. The most direct approach to obtain the radiation pattern is to determine the Poynting vector based on calculating the acceleration fields in the far field and from it the angular distribution using Larmor relations when $\beta \equiv \boldsymbol{v}/c << 1$:

$$\frac{dP}{d\Omega} = \frac{e^2}{4\pi c^3} \left\{ \frac{d\boldsymbol{v}(t)}{dt} \right\}^2 \sin^2\theta \quad \text{and} \quad P = \frac{2}{3} \frac{e^2}{c^3} \left\{ \frac{d\boldsymbol{v}(t)}{dt} \right\}^2 \quad (1)$$

where P is the power, θ is the angle between the observation direction $\boldsymbol{n}$ and the direction of acceleration at emission time t, and c is the light velocity in free space. A straightforward application of Eq. (1) was given in Eq. (1) of Ref. [1] where we noted that a beam of free electrons in an undulator that provides a sinusoidal magnetic field with wavelength λ_U would produce harmonics q of the device wavelength:

$$\lambda \sim \frac{\lambda_U}{2q\gamma^2} \quad (2)$$

where the electron energy γ is in units of rest mass mc^2. Thus one can increase γ or reduce λ_U or the effective mass m *. For low-energy, conduction-band electrons, $\gamma \sim 1$ so that a wiggle period of $\lambda_U = 60\,\mu m$, achievable with standard IC techniques, might be expected to give $30\,\mu m$, 10 THz radiation with angular spread of $1/\gamma$ or 1 radian.

Nomenclature

In a typical, 2-port, passive, microwave structure, the power dissipated (normalized to the input power) can be estimated on the assumption that the S-matrix is complex and orthogonal as:

$$P_l = 1 - |S_{11}|^2 - |S_{21}|^2 \geq 0. \quad (3)$$

The power dissipated can be due to radiation, conductor or substrate loss. For instance, for a standard radiating structure with no output port ($S_{21}=0$), the dissipated power is dependent on S_{11} only so that small values of S_{11} indicate high loss. Further, we assume

that the conductor and substrate loss are much less than radiation loss. The radiated power in this case goes inversely as $|S_{11}|^2$. One can then define the radiation efficiency which is verified by the calculations here as:

$$\eta = \frac{P_l}{P_t} \qquad (4)$$

where P_t is the total power applied to the structure-ideally the so-called wall-plug power that we typically take as 1W.

Finite Difference Time Domain (FDTD) is a powerful and flexible technique that is expected to play a central role in development and simulation of sub-millimeter wave devices [5]. It is ideal for our problem where future research may include anisotropies and nonlinearities, and where high pulsed currents are important. Figure 1 gives sample comparison curves between the FDTD codes developed in this paper and HFSS for the radiation efficiency. These results are obtained from simulating the structure shown in Fig. 6 with dimensions indicated in the caption. In Fig. 1, the radiation efficiency is estimated using two different approaches, i.e. FDTD calculations based on Eqs. 3 and 4 and the integration of far-field-poynting vector using HFSS. Fig. 1 also validates Eq. (3).

Radiation Calculations

Detailed HFSS simulations were carried out to calculate the radiation patterns for several configurations. The half-period layout and radiation pattern for $\varphi=90°$ (the YZ plane) is shown in detail in Fig. 2 for different frequencies. One observes that higher frequencies have higher radiated power while S_{11} trends higher and S_{21} decreases with frequency. Further, at higher frequencies and still looking at the YZ plane, the 90° turns that were put in to avoid crosstalk between input and output ports as well as a well-defined loop, begin to be resolved. They can be viewed as two dipoles at 90° to one another, which become dominant at the highest frequency in Fig. 2 producing the double-lobed distribution. As discussed above these lobes show an expected angular spread of ~$1/\gamma$ or about 1 radian. HFSS simulations were then carried out to calculate the radiative characteristics of Fig. 3 when T=0.0 as shown in Fig. 4 (for $\varphi=90°$). In Fig. 4 at $f = 4.0$ THz, one sees that the radiation comes out predominately perpendicular to the surface and is more symmetric and dipole-like in contrast to the original example (Fig. 2) - especially at 4.2 THz, where the radiation pattern was more diffuse with worse directivity. Also, one observes the usual tradeoffs between radiation efficiency and directivity.

Case 1: Two-Loop, One-Period N=1, d=W Examples

In this section, a second half circle is added to the first one on the same transmission line, with one facing up and the other down but with the tuning distance $d = W$ in Fig. 6. Fig. 5 shows the radiation efficiency versus frequency for three different cases, where Case 3 rearranges the ports to eliminate the 90° turns used in all previous cases. The radiation efficiency is increased over the one-loop examples, e.g. Case 1, because there are two half-circles radiating instead of one but this is mediated by several competing effects. First, because the one-loop case has different (higher) resonant frequencies, the power is superficially lower in Fig. 5. As a result, the background level follows a more obvious quadratic dependence on frequency. Still, comparing Cases 1 and 3, where there is less resonant structure than for Case 2, there is parabolic structure in both curves albeit most clear at the lower frequencies. Using these trends, shifting the curves to compare comparable resonances and averaging gives a crude power doubling between the one and

two loop cases at intermediate frequencies. Similarly, comparing Cases 2 and 3 for the two, double-loop cases, we see nearly perfect interference doubling of the power at the lowest two, strong resonances but which gets successively worse with increasing frequency as the characteristic size of the radiator comes into match with the radiated wavelength.

Case 2: Two-Loop, One-Period N=1 with Different Separation Distances

Fig. 6 shows a top-view of the simulated structure. The main idea is to achieve a constructive radiation of the two-half circles, using d as a tuning element to obtain higher radiated power or radiation efficiency as well as directivity. In order to do this, a transmission line of distance d or some functional equivalent such as multi-port feeds is inserted between the two half-circles. By changing the distance d, the phase difference of the EM-waves propagating along the two half circles is controlled. It is important to mention that the radiated power will be a function of only the frequency f and the distance d when keeping all the other parameters, e.g. the shape, fixed. FDTD simulation results are shown in Fig. 7, where we observe that the cases for $d=0.5R$ and πR correspond most closely to Case 2 of Fig. 5, except that the quadratic variation with frequency is more obvious in Fig. 7. Although the $d=\pi R$ resonance near 16 THz has high efficiency and narrow bandwidth, the peak-to-valley ratio, efficiency, and width of the $d=2R$ resonance at 18 THz is more remarkable. In this case, the circles are the tuning elements for the 90º turns spaced at 2R.

Conclusion and Future Research

We present electromagnetic simulations for various new on-chip THz configurations. Interference effects were studied in terms of both structural shape and tuning parameters to improve output intensity, bandwidth and directionality. Results imply that we can design an efficient THz radiator by tuning the phases of the EM-waves propagating from the different sections of the structure. Results are validated by comparing two independent calculations from the developed FDTD code and a commercial finite-element code (HFSS) [6] that agreed quite well. Our main goal in this paper was to concentrate on the radiative characteristics and determine whether the underlying electromagnetics we were assuming were sound. Clearly, there are some very important questions to be pursued on the physical device side--some of which are quite fundamental. On the production side, depending on the option, the challenges don't lie in the feature sizes but in the materials and operating conditions such as the excitation or drive source, ballistic transport conditions, and replenishing the pulse current and voltage as the radiation process proceeds at high efficiency.

REFERENCES

[1]   Y. A. Hussein and J. E. Spencer, "Novel possibilities for coherent radiation sources," in *2004 IEEE MTT-S Int. Sym. Dig.*, to be published.
[2]   P. H. Siegel, "Terahertz technology in biology and medicine," *IEEE Trans. Microwave Theory Tech.*, vol. 52, No. 10, pp. 2438-2447, Oct. 2004.
[3]   S. J. Allen, "Terahertz dynamics in semiconductor quantum structures,"*27th Int'l. Conf. Infrared and Millimeter Waves*, Sept. 2002.

[4]   The Stanford HEPLs FIREFLY undulator typically produces ≤ 1 W of 15-85 µm radiation with a 30 MeV superconducting linac while FELIX in the Netherlands produces 20-250 µm at comparable power.

[5]   A. Taflove, *Computational Electrodynamics: The Finite-Difference Time-Domain Method.* Norwood, MA: Artech House, 1995.

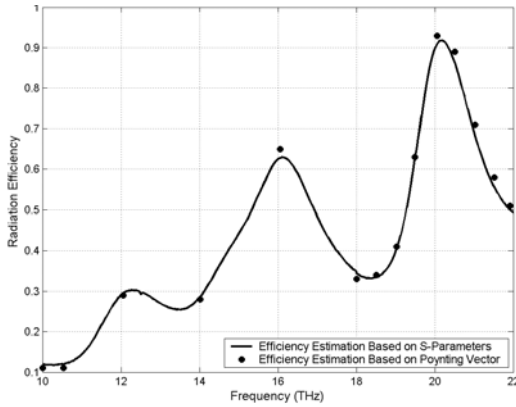[6]   Ansoft Corporation high frequency structure simulator (HFSS), version 9.0 for Windows, released May 2003.

Fig. 1. Radiation efficiency comparisons for the structure shown in Fig. 6 when d=W and R=3.6 µm.

Fig. 2. Radiation pattern for the total electric field at $\varphi = 90°$ for different frequencies where the radial scale is in V/m for a normalized input of 1 W.
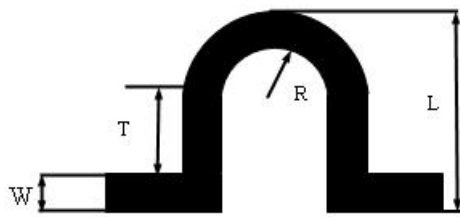
Fig. 3. Top-view of the 0.5 period case (not to scale). R = 4 μm, W = 2 μm, and T = 0, 2, and 3.2 μm.
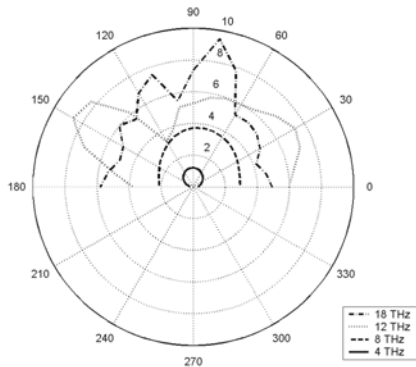
Fig. 4. Radiation pattern for the total electric field at φ=90° for different frequencies.

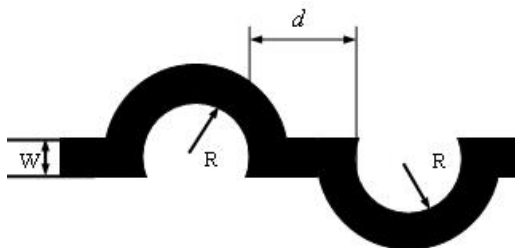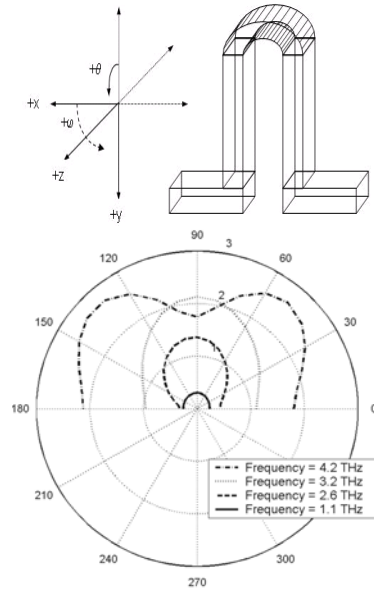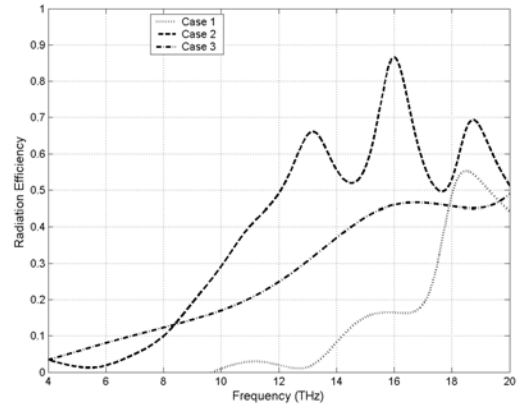Fig. 5. Radiation efficiency curves for three cases (d=W). Case 1: single half-circle. Case 2: two half-circles. Case 3: two half-circles without 90° turns based on rearranging ports.
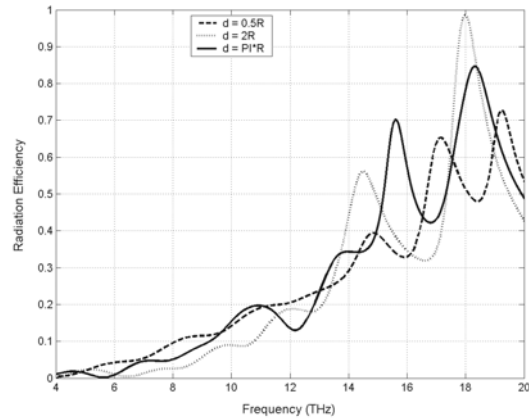

Fig. 6. Top-view of two half-circles (not to scale) separated by a distance d. R = 4 μm and W= 2 μm.

Fig. 7. Radiation efficiency curves for different values of the separation distance d.